Alma Mater Studiorum Università di Bologna
Archivio istituzionale della ricerca

Inkjet-Printed Carbon Nanotube Electrodes Modified with Dimer-captosuccinic Acid-Capped Fe3O4 Nanoparticles on Reduced Graphene Oxide Nanosheets for Single-Drop Determination of Trifluoperazine

19 February 2025

Inkjet-Printed Carbon Nanotube Electrodes Modified with Dimercaptosuccinic Acid-Capped Fe₃O₄ Nanoparticles on Reduced Graphene Oxide Nanosheets for Single-Drop Determination of Trifluoperazine

Miloš Ognjanović,* Dalibor M. Stanković, Milica Jović, Milena P. Krstić, Andreas Lesch, Hubert H. Girault, and Bratislav Antić

ABSTRACT: Here, we report the design of a disposable single-drop voltammetric sensor for the quantitative determination of antipsychotic drug trifluoperazine (TFP). The sensor was built using inkjet-printed carbon nanotube (CNT) electrodes, which were modified with dimercaptosuccinic acid (DMSA)-coated magnetite nanoparticles uniformly dispersed over reduced graphene oxide nanosheets (DMSA/Fe₃O₄/RGO). The used modifying materials were characterized by electron microscopy techniques (transmission electron microscopy (TEM) and field emission-scanning electron microscopy (FE-SEM)), X-ray powder diffraction, ζ-potential measurements, dynamic light scattering (DLS), and electrochemical methods (cyclic voltammetry (CV) and electrochemical impedance spectroscopy (EIS)). The developed sensor, best operated at pH 7 in the Britton−Robinson buffer solution (BRBS), shows linear electrocatalytic activity with TFP in the concentration range of 1−50 μM, a low detection limit of 0.54 μM, and excellent selectivity, repeatability, and reproducibility with an relative standard deviation (RSD) of 2.4%. A voltammetric approach using square wave voltammetry (SWV) is a sensitive technique under optimized conditions for the analytical determination of submicromolar amounts of TFP. Bare CNT and RGO- and DMSA/Fe₃O₄-modified CNT electrodes showed lower electrocatalytic activity than the DMSA/Fe₃O₄/RGO/CNT electrode. The development of this kind of TFP sensor based on nanoparticle-decorated graphene nanosheets can offer a tool for point-of-care applications as sensors in biomedicine.

KEYWORDS: *disposable sensor, magnetite, graphene nanocomposite, square wave voltammetry, CNT electrodes*

INTRODUCTION

Trifluoperazine (10-[3-(4-methyl-1-piperazinyl)propyl]-2-(trifluoromethyl)-10*H*-phenothiazine, TFP) is a dopamine antagonist with antipsychotic and antiemetic activities mainly used for schizophrenia treatment.[1] TFP is one of the most potent antipsychotic phenothiazine-type drugs that express its antipsychotic effect by blocking central dopamine receptors and prevent effects such as delusions and hallucinations caused by an excess of dopamine. This agent also functions as a calmodulin inhibitor, thereby leading to an increase of cytosolic calcium. Trifluoperazine was also reported to be superior as a placebo for the treatment of generalized anxiety disorder[2] and as an inhibitor of cancer stem cell growth.[3] As TFP is highly metabolized by the liver and eliminated in the urine, there has been a need for a new method for the detection of this drug in biological fluids and pharmaceuticals. Considering the structure of trifluoperazine (Scheme 1), its electrochemical nature should be distinctively determined by the phenothiazine core and the appointed piperazine ligand.[4]

The clinical method for TFP determination by the United States Pharmacopeia is volumetric nonaqueous titration with perchloric acid, which requires a large number of drug samples and organic solvents.[5] Considering the electrochemical methods, which can have a significant impact on this area, only a few have been reported so far, based on boron-doped diamond electrode,[6] poly-aminobenzene sulfonic acid/single-walled carbon nanotubes (CNTs) composite-modified glassy carbon electrode,[7] multiwalled carbon nanotube-modified glassy carbon,[8] and aminobenzene sulfonic acid/single-wall carbon nanotubes/glassy carbon electrode.[9] The main aim of

Scheme 1. 10-[3-(4-methyl-1-piperazinyl)propyl]-2-(trifluoromethyl)-10H-phenothiazine (TFP)
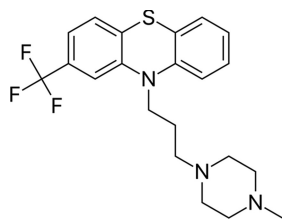
this work was to design a new droplet-based electrochemical sensor based on graphene (GR) nanocomposite with improved performances toward TFP determination. Nanoparticle-decorated graphene was frequently used for surface modification of the working electrode (WE) in building new sensors.[10]

Functionalized graphene materials have attracted much attention in electrochemical sensors due to their exciting properties such as high surface area and electron transport under ambient conditions, which make them promising candidates for implementation in portable sensors.[11,12] Graphene (GR), a flat monolayer of sp^2-bonded carbon atoms tightly packed into a two-dimensional honeycomb lattice, is considered as one of the thinnest materials on Earth.[13,14] Graphene oxide (GO) is one of the most important derivatives of graphene and possesses an enormous surface area, reasonable conductivity depending on the degree of oxidation, and great mechanical properties. It is used in various fields such as energy materials, biosensing, catalysis, and biomedicine.[15] Furthermore, it is difficult to disperse GR in polar solvents due to its hydrophobicity. On the other hand, GO contains hydrophilic groups, such as $-OH$, $-COOH$, $-O-C=O$, and $=C=O$, and can, therefore, be homogeneously dispersed together with active materials, like commonly used metal oxides, in a polar matrix for its deposition onto the electrode surfaces. In GO, the π-network, and thus the electronic conductivity, is lower compared to that of GR. Therefore, GO cannot be directly used as a conductive electrode material because it needs to be reduced to reduced graphene oxide (RGO) under regeneration of the π-network.[16] On the other hand, the research on magnetic nanomaterials, especially iron oxide nanoparticles (IONPs), constitute one of the most dynamic and fast-growing areas of research in the field of nanotechnology.[17−19] The properties of IONPs differ significantly from those of the iron oxide bulk counterpart and depend on several factors such as composition, surface area, shape, size, surface morphology, and anisotropy. Among the possible materials for the surface modification of IONPs, dimercaptosuccinic acid (DMSA), a small organic molecule, has been widely used to form aqueous suspensions and provide better dispersity of nanoparticles and consequently a higher surface area.[20] Furthermore, the decoration of graphene-based materials by bare or surface-modified IONPs has become a hot topic due to their enhanced functionalities.[21,22] The graphene-based nanocomposites fabricated by this way hold a great promise for designing an electrochemical sensor that has a wide variety of applications in biomedical fields, catalysis, removal of contaminants from wastewater, biosensors, etc.[23−25] The achieved functionalities are due to the combined or synergistic effect of enhancing electron transfer rates and active surface conductivity by increasing the specific surface area and promoting transition.

Disposable inkjet-printed carbon nanotube electrodes are a recently developed type of electrode with many desirable properties like high conductivity, droplet detection, small active area, and good mechanical strength of the employed CNTs,[26−28] which make them attractive for use in flexible nanoelectronic devices.[29] After modification of the CNT patterns with other carbon-based nanocomposites, the CNT electrode performance could be further improved so that the inkjet-printed CNT electrodes have the potential to be a great starting point for the production of small flexible sensors for point-of-care (POC) electronic devices.[30,31]

Herein, we report the fabrication and application of a sensitive and highly selective disposable droplet-based electrochemical sensor for the detection of TFP in biological fluids. Uniform iron oxide magnetic nanoparticles with a controlled core diameter of 13 nm have been synthesized by thermal decomposition of an iron oleate complex in 1-octadecene. The synthesized nanoparticles were coated with DMSA for better dispersibility in polar solvents and spread over the sheets of reduced graphene oxide (DMSA/Fe_3O_4/RGO). The proposed nanocomposite was further used for the modification of inkjet-printed CNT electrodes and applied for the detection of TFP.

EXPERIMENTAL SECTION

Reagents. All reagents were used as obtained and without any further treatment. For the synthesis of nanocomposite DMSA/Fe_3O_4/RGO commercial products, iron(III) chloride hexahydrate (98%, Sigma-Aldrich), sodium oleate (82%, Riedel-de Haen), oleic acid (90%, Aldrich), 1-octadecene (90%, Sigma-Aldrich), n-hexane (99%, Scharlau), toluene (99.8%, Sigma-Aldrich), meso-2,3-dimercaptosuccinic acid (DMSA, ∼98%, Sigma-Aldrich), dimethyl sulfoxide (DMSO, ≥99%, Sigma-Aldrich), graphene oxide sheets (Sigma-Aldrich), ethylene glycol (≥99.5%, Fluka Analytical), and ammonium hydroxide solution (28% NH_3 in H_2O, ≥99.99%, Sigma-Aldrich) were used. The following materials were used for the fabrication of inkjet-printed carbon nanotube electrodes: disposable ink of nanosilver (Silverjet DGP-40LT-15C; w/w 30−35%, Sigma-Aldrich), CNT dispersion (Brewer Science), jettable insulator EMD6201 (Sun Chemical), and hypochlorite solution (Acros Organics; available chlorine, 5%).

Synthesis of DMSA/Fe_3O_4/RGO Nanocomposite. Uniform iron oxide magnetic nanoparticles were synthesized by the thermal decomposition of an iron oleate complex in 1-octadecene by controlling the nucleation and growth processes using the slightly modified procedure described in ref 32. Briefly, the iron oleate complex was synthesized by measuring 45 g of sodium oleate and 10.8 g of $FeCl_3$6H_2O and mixing them with distilled water (60 mL), absolute ethanol (80 mL), and n-hexane (140 mL) inside a one-neck round-bottom flask. The suspension was heated for 4 h at 70 °C under magnetic stirring, and after cooling to room temperature (RT), the solution was poured into a separation funnel and the phases were separated by washing with a mixture of ethanol and water. Once the washing procedure has been completed and the last aqueous layer was removed, the top layer containing the iron oleate complex was transferred to the single-neck round-bottom flask. All of the solvents were removed using a rotary evaporator. An amount of iron oleate complex (4.5 g) prepared in the previous section was transferred to a three-neck round-bottom flask, mixed with 50 mL of 1-octadecene, and placed on an electric mantle under mechanical stirring with a nitrogen atmosphere. The temperature program was set to reach 315 °C (±5 °C), maintained for 1 h, and allowed to decrease to RT. Then, nanoparticles were precipitated with absolute ethanol, centrifuged, and finally dispersed in 25 mL of toluene.

For a better dispersion of the nanoparticles, their surface modification was conducted according to the procedure described in ref 33. The nanoparticles were coated with DMSA by mixing 5 mL of a toluene nanoparticle stock with 90 mg of meso-2,3-

Scheme 2. (A) Synthesis of DMSA/Fe$_3$O$_4$/RGO Nanocomposite and Modification of CNT Electrode. (B) Schematic Illustration of CNT Electrode (QRE, WE, and CE Denote Quasi-Reference Electrode, Working Electrode, and Counter Electrode, Respectively). (C) Photographs of Three Modified Electrodes by Drop-Casting 2 μL of Materials on the Working Electrode
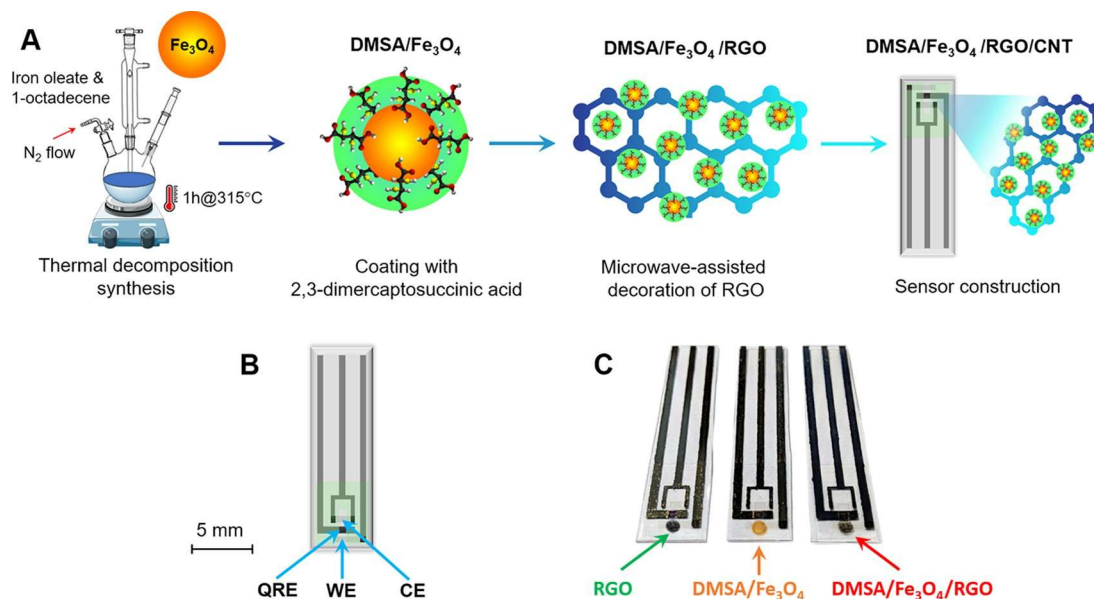
dimercaptosuccinic acid and 5 mL of dimethyl sulfoxide, followed by 10 min processing in an ultrasonic bath. The system was placed on a rotator, and the solution was mixed at 10−20 rpm for 48 h. The supernatant was decanted, and the precipitate was centrifuged, washed three times with ethanol, and allowed to dry for 24 h in air.

In the last step of the nanocomposite synthesis, DMSA-coated iron oxide nanoparticles were used for decorating graphene oxide (GO) sheets. For this, 5 mg of the synthesized iron oxide nanoparticles were mixed with 1.5 mL of GO suspension (5 mg·mL^{-1}) in 25 mL of ultrapure Milli-Q water under 4 h of magnetic stirring to achieve a uniform suspension. The pH value of the suspension was adjusted to about 10 by the addition of NH$_4$OH. After that, the mixture was sonicated for 1 h at RT. Then, the suspension was heated at 160 °C for 10 min using a microwave synthesis reactor (Anton Paar, Monowave 300, Austria), followed by cooling inside of the reactor to RT. The black precipitate was centrifuged, washed with deionized water several times, and finally redispersed in 5 mL of dimethylformamide (DMF). For the sake of comparison, RGO was also obtained by reduction from GO by direct microwave-assisted irradiation. It has been shown that GO can be reduced to RGO by microwave irradiation.[34] The process of nanocomposite synthesis is shown graphically in Scheme 2A.

Characterization Techniques. The crystal structure properties were analyzed using X-ray powder diffraction (XRPD) data. The measurements were performed on a high-resolution SmartLab X-ray diffractometer (Rigaku, Japan) equipped with a Cu Kα radiation source (λ = 0.1542 nm). The collected data were in the 2θ range of 10−75° with the following conditions: a step of 0.05°, exposition of 2 s per step, divergent slit of 0.5 mm, and operating at 40 kV and 30 mA.

The microstructure and morphology of the synthesized samples were investigated using a transmission electron microscope (TEM) JEOL-JEM 1010 (JEOL, Japan) operating at 100 kV and a field emission scanning electron microscope field emission-scanning electron microscopy (FE-SEM) MIRA3 (Tescan, the Czech Republic) operating at 30 kV. The sample was prepared by placing a drop of particles suspended in water onto a carbon-coated copper grid and allowing it to dry at RT for FE-SEM and TEM observations. The TEM images were analyzed manually by ImageJ software.[35] The mean particle size and distribution were evaluated by measuring the largest internal dimension of 300 nanoparticles. Afterward, the data

were fitted to a log-normal function to obtain the mean size and

$$y = y_0 + \frac{A}{\sqrt{2\pi}\omega x}e^{-[\ln x/xc]^2/2\omega^2}$$

standard deviation (σ) as well as the index of polydispersity (PdI), which is considered to denote the absolute error of the measurement.

The ζ-potentials of a 0.1 mg·mL^{-1} suspension of naked and DMSA-coated samples dispersed in deionized water were measured at 25 ± 0.1 °C in disposable zeta cells (DTS 1070) of a NanoZS90 (Malvern, U.K.) device. The samples were used after 30 min of equilibrium at a constant ionic strength of 0.01 M set by NaCl. The hydrodynamic particle size was determined by dynamic light scattering (DLS) on a NanoZS90 apparatus (Malvern, U.K.) with a 4 mW He−Ne laser source (λ = 633 nm). The stock sols of two samples were diluted to a concentration of 0.1 mg·mL^{-1}. The pH was varied between 2 and 12 by the addition of HNO$_3$ and KOH. All measurements were performed at a given kinetic state, followed by a minute of relaxation. The average values of the hydrodynamic diameter were calculated as the number weighted size from fits of the correlation functions. pH measurements were performed using a Lab pH Meter inoLab (WTW, Germany) with a combined glass electrode (SenTix 41).

Electrochemical experiments were executed using Autolab potentiostat model 302 N (Autolab PGSTAT302N, Metrohm, the Netherlands) in a three-electrode arrangement system with a working electrode (WE), a counter electrode (CE), and a reference electrode (RE). The experiments were performed in a 0.1 M Britton−Robinson buffer solution at pH 7. Electrochemical impedance spectroscopy (EIS) measurements were performed in the presence of a stationary 5 mM K$_3$[Fe(CN)]$_6$/K$_4$[Fe(CN)]$_6$ (1:1) mixture as a redox probe in a 0.1 M KCl solution with the frequency changed from 100 Hz to 100 kHz with a signal amplitude of 5 mV at a potential of 0.05 V. The scan rate in cyclic voltammetry (CV) was 50 mV·s^{-1}.

Fabrication of Inkjet-Printed Carbon Nanotube (CNT) Electrodes and Modified CNT Electrodes. Inkjet-printed carbon nanotube electrodes were produced on PET substrates (thickness, 180 μm) based on a protocol precisely described elsewhere.[36−38] Briefly, the electrodes were printed using an X-Serie inkjet-printer (CeraDrop, France) equipped with piezoelectric Dimatix Q-class Sapphire QS-256/80pL print-heads and disposable DMC-11610 cartridges. As a first layer, jettable nanosilver ink was inkjet-printed and cured as an electrical connection layer and quasi-reference electrode

material. The second printed material was a CNT dispersion used for the fabrication of CNT patterns to form stand-alone working and counter electrodes. The third layer was a dielectric ink that was inkjet-printed and, at the same time, UV-photopolymerized, forming an insulation layer on top of the silver-lines and specifically defining all operating electrode surface areas (WE-CNT, QRE-Ag, CE-CNT) of about 1 mm^2 each. Finally, the silver electrode was chemically converted into a Ag/AgCl quasi-reference electrode by exposing the silver electrode surface to a hypochlorite solution and finally washing with water.[38,39] The graphical illustration of the CNT electrode and the photographs of already prepared sensors are given in Scheme 2. A more in-depth schematic layer-by-layer description of CNT electrodes can be found in detail in our previous works.[31,36] Briefly, it is presented in Scheme 2B.

To prepare DMSA/Fe$_3$O$_4$/RGO/CNT electrodes, the synthesized DMSA/Fe$_3$O$_4$/RGO powder was dried, dissolved in DMF (5 mg· mL^{-1}), and sonicated for 3 h. After this period, 2 μL of the composite solution was deposited on the carbon nanotube working electrode (WE-CNT) and allowed to dry at RT. DMSA/Fe$_3$O$_4$/RGO/CNT electrodes were further dried overnight at +4 °C. As working electrodes, bare CNT and DMSA/Fe$_3$O$_4$-, RGO-, and DMSA/Fe$_3$O$_4$/ RGO-modified CNT electrodes were used and compared.

Samples for Testing Modified CNT Detection of TFP. Human urine samples were obtained from four healthy and young people (female and male). The urine samples were prepared according to our previous work.[40] Before use, the samples were stored in a refrigerator at +4 °C and spiked with a standard solution of TFP on the day of measurement. Additionally, blood serum samples of two healthy volunteers were acquired from a local hospital. After centrifugation, 1 mL of the supernatant was added to 0.8 mL of acetonitrile and stirred for 45 s. The obtained mixture was centrifuged at 15 000 rpm for 10 min. After centrifugation, different volumes of the obtained supernatant were directly analyzed. The samples were spiked with a standard solution of TFP. Recovery studies for both urine and blood serum were carried out. Results are calculated from the calibration curve and summarized as a mean value of three independent measurements.

RESULTS AND DISCUSSION

Structural Characterization of Nanoparticles and Nanocomposite. The crystal structure and microstructure of magnetite nanoparticles and nanocomposite were examined by X-ray diffraction and electron microscopy techniques (TEM and FE-SEM). Thanks to the thin DMSA surface layer surrounding the nanoparticles, the particles were less agglomerated and thus well dispersed. The TEM micrographs of the synthesized nanoparticles are shown in Figure 1A. As illustrated, these nanoparticles were mainly spherical, well dispersed, and uniform in size, d_{TEM} = 13.1 ± 0.8 nm. The nanoparticles undergo log-normal size distribution with a PdI index of 6.4% (Figure 1B). The surface morphology of GO and DMSA/Fe$_3$O$_4$/RGO was observed using FE-SEM. Figure 1C reveals an almost transparent single layer of GO, which possesses a large surface area. There are many wrinkles and creases on the folded surface of GO to reduce the surface energy making it more stable. Small magnetite nanoparticles are scattered over the surface of RGO sheets, further enhancing the surface area, as displayed in Figure 1D. These results indicate that the nanoparticles are firmly and homogeneously dispersed to the RGO nanosheets with a vital influence on the surface of the nanocomposite that was beneficial for the electrochemical processes (see below).[41,42] The crystal structures of DMSA/Fe$_3$O$_4$, GO, RGO, and DMSA/Fe$_3$O$_4$/RGO were checked by X-ray powder diffraction (Figure 2A). The reflections of the synthesized DMSA/ Fe$_3$O$_4$ (orange line) can be ascribed to the spinel structure
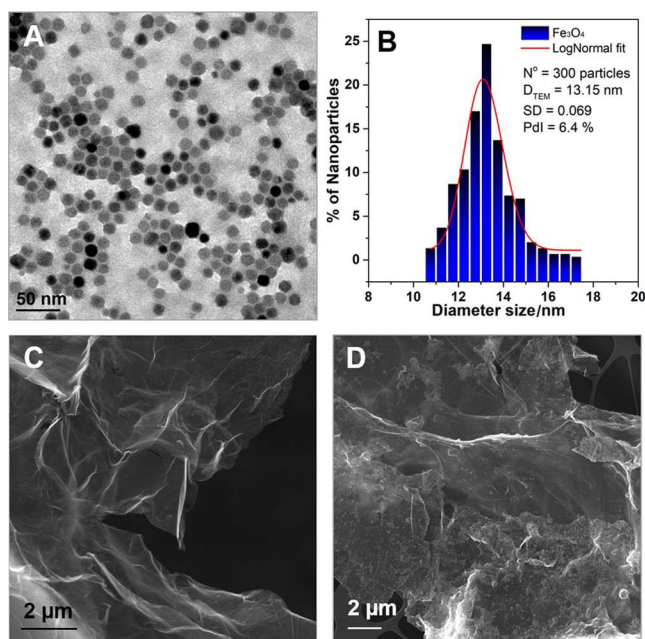

Figure 1. (A) TEM micrograph of DMSA-coated Fe$_3$O$_4$ nanoparticles; the scale bar is 50 nm. (B) Log-normal size distribution of iron oxide nanoparticles. FE-SEM micrographs of (C) GO and (D) DMSA/Fe$_3$O$_4$/RGO nanocomposite.

type, space group $Fd\overline{3}m$ (No. 227), matching the most intensive diffraction peaks with the simulated diffraction data (JCPDS card #19-629). The crystallite size estimated by the Debye−Scherrer equation of the most intensive reflection (311) gave the result of d_{XRPD} = 9.49 nm and agreed well with d_{TEM}, suggesting the high crystallinity of the nanoparticles. The sharp diffraction peak at 10.25° matched well with the (002) reflection of GO (blue line). This peak turned into a broad peak at 2θ = 22.5° after the microwave synthesis (green line). This is a confirmation of the successful reduction of GO to RGO.[43] Accordingly, the XRPD pattern of DMSA/Fe$_3$O$_4$/ RGO (red line) suggests that in the course of the microwave-assisted hydrothermal synthesis, highly dispersed nanocrystals of Fe$_3$O$_4$ become anchored to the RGO sheets generated from the GO reduction during synthesis. RGO sheets were generated from the GO reduction during the synthesis.

A well-established method for the surface modification of nanoparticles should determine if the coating procedure is performed successfully. The constructed ζ-potential vs pH curves for uncoated and DMSA-coated Fe$_3$O$_4$ NPs are shown in Figure 2B. The successful coating process can be confirmed by the reduction of the isoelectric point (the point of zero charge of the particles) from pH 7.6 to pH 3.6 and by a slight reduction of the surface charge. The addition of the carboxylic group-rich dimercaptosuccinic acid to the suspension of Fe$_3$O$_4$ that is rich in positive ions of Fe$^{2+/3+}$ on the surface NPs had an apparent effect on the ζ-potential of the nanoparticles, making the dispersion more stable at physiological pH. The Coulomb electrostatic repulsion forces are key to the assembly process and DMSA/Fe$_3$O$_4$ coating. The effect of coating procedure on the hydrodynamic size (D_H) of particles, measured by DLS, is shown in Figure 2C. The D_H values increased from 20.8 nm for naked Fe$_3$O$_4$ to 46.9 nm for DMSA-coated Fe$_3$O$_4$ nanoparticles, which showed that the outer shell of dimercaptosuccinic acid is stacked over magnetite nanoparticles. It must be noted that D_H represents the diameter of particles in their
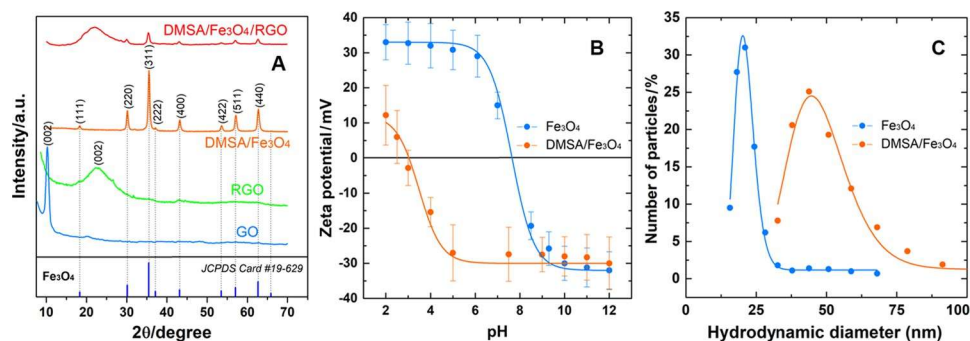
Figure 2. (A) XRPD patterns of the synthesized samples: GO (blue line), RGO (green line), DMSA/Fe$_3$O$_4$ nanoparticles (orange line), and DMSA/Fe$_3$O$_4$/RGO composite (red line). For comparison, a typical Fe$_3$O$_4$ pattern (JCPDS card #19-629) is also displayed. (B) Effect of pH on the ζ-potential of naked and DMSA-coated Fe$_3$O$_4$ nanoparticles. (C) Hydrodynamic diameter of uncoated and coated nanoparticles.

hydrated state in water dispersion and that its value is higher than d_{TEM}, which represents the diameter of particles itself.

Electrochemical Performance of the Proposed Sensor. The electrocatalytic activity of unmodified and modified CNT electrodes toward the electrochemical detection of 75 μM of TFP was examined using cyclic voltammetry of the Britton−Robinson buffer solution (BRBS) at pH 7 with a scan rate of 50 mV·s^{-1}. Figure 3A shows changes in oxidation
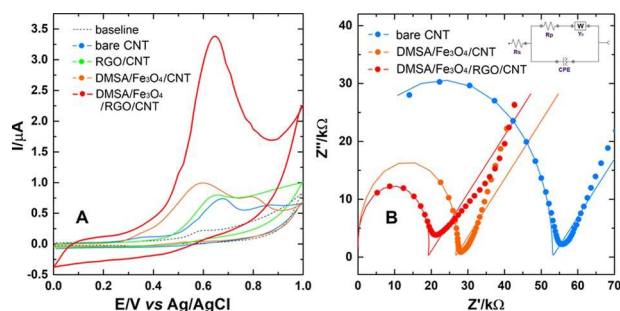

Figure 3. (A) Electrochemical response of TFP (75 μM) at bare CNT and DMSA/Fe$_3$O$_4$-, RGO-, and DMSA/Fe$_3$O$_4$/RGO-modified CNT electrodes. Supporting electrolyte BRBS at pH 7; scan rate, 50 mV·s^{-1}. (B) Nyquist plots for various electrodes, bare CNT, and RGO- DMSA/Fe$_3$O$_4$-, and DMSA/Fe$_3$O$_4$/RGO-modified CNT. Inset: Equivalent circuit for the electrochemical impedance spectroscopy data. The frequency range was from 100 Hz to 100 kHz.

currents that display electrocatalytic behavior of bare and differently modified CNT electrodes. As it can be seen, TFP shows an oxidation peak with an $E_{1/2}$ potential of around 0.63 V. The RGO-modified CNT electrode (green line) increased the oxidation peak of the CNT electrode (blue line) from 0.75 to 0.8 μA, while the DMSA/Fe$_3$O$_4$-modified CNT electrode (orange line) increased the current to 1 μA. The experimental result shows that when DMSA/Fe$_3$O$_4$/RGO was deposited over the CNT electrode (red line), the current increased more than four times, which could be due to a faster electron transfer rate. This can be attributed to the increasing capability of diffusion and active surface area of the electrode. The use of the inkjet-printed CNT electrode was beneficial due to the miniaturized sensor dimensions compared to the standard screen-printed carbon electrode (SPCE), which resulted in 25 times lower amounts of analyte per analysis (as low as 2−5 μL^{-1}).[31]

To investigate the electron transfer capabilities of different electrodes, AC impedance experiments were carried out. EIS measurements were performed since EIS is an effective and sensitive tool for the characterization of the interface properties of an electrode surface during each modification step. The obtained Nyquist diagrams at the different electrodes are shown in Figure 3B. In the Nyquist plot, the electron transfer resistance (R_{ct}) on the sensor surface is related to the diameter of the semicircle. According to the results, the bare CNT electrode showed the highest semicircle diameter. A resistance value higher than 55 kΩ indicates a slow electron transfer process for 5 mM Fe(CN)$_6^{3-/4-}$ as a redox probe. The smallest semicircle diameter at ∼20 kΩ of the DMSA/Fe$_3$O$_4$/RGO/CNT indicated that the modification of the CNT layer with DMSA/Fe$_3$O$_4$/RGO decreased the electron transfer resistance of the interface. On the other hand, a large R_{ct} value for DMSA/Fe$_3$O$_4$/CNT of about 28 kΩ, and 50 kΩ of RGO/CNT indicated that the combination of RGO and Fe$_3$O$_4$ on the sensing surface was essential for good sensor performance. The experimental impedance data were further fitted using an equivalent electrical circuit fit tool in the NOVA 2 software package (Metrohm Autolab). Several models of circuits to fit our experimental data were attempted. The best results (best agreement between experiment and fitting for all three electrodes) were obtained with the equivalent circuit presented as an inset of Figure 3B.

The dynamic surface area of bare and modified electrodes was calculated using the Randles−Sevcik equation. The CV technique was used to measure 1.0 mM K$_3$[Fe(CN)$_6$] as a test analyte, and 0.1 M KCl was used as the supporting electrolyte at different scan rates at 25 °C (Figure S1). Equation 1 was used to calculate the surface area of the electrode

$$I_p = (2.69 \times 10^5)n^{3/2}AD_0^{1/2}v^{1/2}c_0^* \quad (1)$$

where n is the number of electrons involved in the reaction, i.e., equal to 1, A is the effective area of the electrode, D_0 is the diffusion coefficient (7.6×10^{-6} cm^2·s^{-1} for K$_3$[Fe(CN)$_6$]), v is the scan rate, and c_0^* is the concentration of K$_3$[Fe(CN)$_6$] (1.0 mM). From the slope of the plot, $I_p = f(v^{1/2})$ the effective surface area of the bare electrode was found to be 0.041 cm^2 for unmodified CNT electrode and the effective area for the DMSA/Fe$_3$O$_4$/RGO/CNT was more than five times larger (0.285 cm^2). The TFP can lose two electrons in the oxidation process. If two electrons were lost together in two steps, there were two anodic peaks, like in the case of bare CNT electrode. But under the condition with DMSA/Fe$_3$O$_4$/RGO nanocomposite, apparently, two electrons were lost in one step, and thus only one peak appeared.[7]

Selection of the pH of the Supporting Electrolyte and Investigation of the Effect of Scan Rate. In order to study the effect of the pH of the supporting electrolyte (Figure 4A), cyclic voltammetry was used. A constant increase in peak
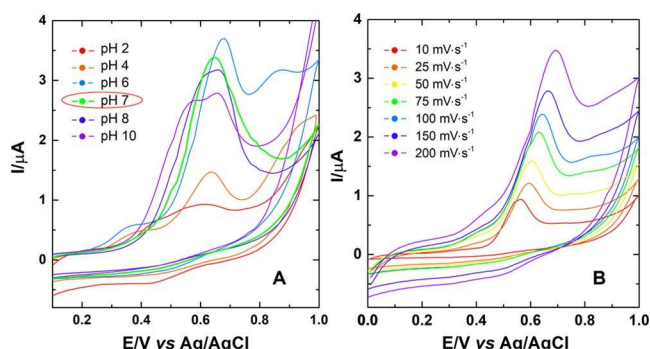

Figure 4. (A) Cyclic voltammograms of TFP (75 μM) at DMSA/Fe$_3$O$_4$/RGO-modified CNT electrode at various pH values of BRBS; scan rate, 50 mV·s^{-1}. (B) Cyclic voltammograms of TFP (75 μM) at DMSA/Fe$_3$O$_4$/RGO-modified CNT electrode at various scan rates. Supporting electrolyte BRBS pH 7.

currents with pH was noted in the Britton−Robinson buffer solution, reaching the maximum at pH 7. Beyond pH 7, the currents slightly decreased, but the spreading of the peaks was also observed. This may be due to the favorable oxidation of resembling molecules in acid environments, by the reaction: R−OH + 2H$^+$ + 2e$^-$ → R−OH$^\bullet$ and the generation of polymeric compounds, typical for polyphenols.[44] Consequently, BRBS at pH 7 was chosen as a basic electrolyte for further experiments. Additionally, cyclic voltammograms of the same concentration of TPF at pH 7 were recorded at various scan rates to examine the nature of the process that takes place at the surface of the modified electrodes (Figure 4B). The increase of the scan rate was followed by an increase in the oxidative peak currents. The peak currents were linearly increasing with the square root of scan rate, as seen in Figure S2A, indicating that the process is diffusion-controlled. The corresponding linear equation for the oxidation process was I (μA) = 0.091$v^{1/2}$ (mVs^{-1})$^{1/2}$ + 0.343, with a regression coefficient of 0.9981. Similarly, the dependency of log I vs log v was linearly described by the equation log I = 0.344 log v − 0.588 and a regression coefficient of 0.9987 (Figure S2B). Given the above results, it was clear that the processes dominant at the working electrode surface are diffusion-controlled. A small movement of the peak potentials could be attributed to the minor contribution of the processes that are controlled by adsorption.

Based on Laviron's theory, the number of electrons involved in the electrochemical oxidation can be calculated using eq 2

$$I_p = n^2F^2vA\Gamma_0^*/4RT = nFQv/4RT \tag{2}$$

From this equation, electron number (n) can be calculated as long as the peak current (I_p) and peak area (Q) are obtained under a certain scan rate (v). According to eq 2, n was calculated to be 1.4, meaning two electrons were involved in the electrochemical oxidation, which is in accordance with other reported values.[7]

Square Wave Voltammetry Detection of TFP. For the quantification of TFP, square wave voltammetry (SWV) was chosen. To increase the sensitivity and selectivity of the

suggested method, different conditions were varied, such as amplitude (tested range, 10−100 mV), frequency (5−50 Hz), and potential step (2−15 mV). While one parameter was varied, the others were kept constant. The obtained optimum values were amplitude, 60 mV; frequency, 5 Hz; and step of potential, 10 mV. The calibration plot was made by the consecutive addition of a TFP standard solution. The SWV response of the DMSA/Fe$_3$O$_4$/RGO/CNT electrode toward different standard solutions of TFP and the corresponding calibration graph are shown in Figure 5A,B, given the linear
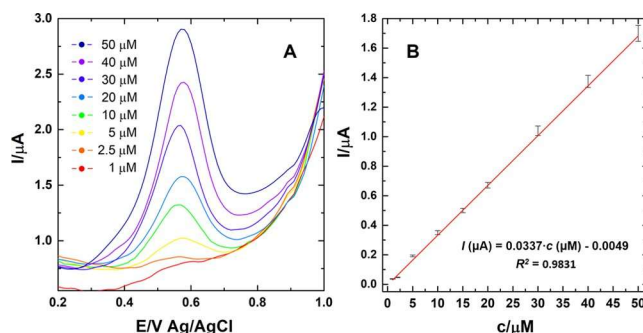

Figure 5. (A) SWV voltammograms obtained with DMSA/Fe$_3$O$_4$/RGO/CNT electrode for the concentration range of TFP from 1 to 50 μM, pH = 7 and (B) the corresponding calibration plot evaluated from the measurements. All experiments were conducted under previously optimized experimental conditions.

range (1−50 μM) of the graph was obtained under optimal conditions. The linear equation of this dependence is I (μA) = 0.0337c (μM) − 0.0049 with a correlation coefficient of 0.9831. The detection limit (LOD, 3 sd$_{intercept}$/slope) of TFP using the DMSA/Fe$_3$O$_4$/RGO/CNT sensor was 0.54 μM, while the quantification limit (LOQ, 10 sd$_{intercept}$/slope) was 1.79 μM. The obtained linear range (0.4−20.4 mgL^{-1}) is well beyond the C_{max} value of TFP (15−20 mg·day^{-1}), which falls into the upper end of our detection limit. The obtained results are comparable to a few alternative sensors found in the literature.[6,7,9] As it can be seen in Table 1, the electroanalytical data of the sensor constructed here were comparable to those of the already reported TFP sensors in biological samples, especially in the linear range. Additionally, using this construction of the working electrode, only one drop (2−5 μL) of sample solution was needed for analysis, which is very attractive for point-of-care applications.

For the determination of the reproducibility of the designed sensor, 10 μM TFP was analyzed with six identically modified electrodes under the same SWV conditions. All of the sensors were stored in a refrigerator at +4 °C for a few days before use. The relative standard deviation (RSD) for the detected peak currents obtained from the measurements was calculated to be 2.4% (n = 6) as an indicator of the sensor's precision (Figure S3 and Table S1). Given these results, the sensor fabrication process is highly reproducible and sensors are successfully used for the determination of TFP concentration.

Interference Analysis and Real-Sample Analysis. Before testing the practical applicability of the proposed method in real samples, the interfering effect of some ordinary compounds, which could be found in biological fluids, was examined. The sensor's selectivity was validated in the presence of ascorbic acid (AA), uric acid (UA), dopamine (DOP), and glucose (Glu), and all four combined (AA + UA +

Table 1. Comparison of the TFP Sensors Reported in the Literature

electrode	detection method	linear range (μM)	detection limit (μM)	refs
BDD[a]	DPV	1−37	0.6	6
ABSA/SWNT/GCE[b]	DPV	0.1−10	0.001	7
MWCNT/GCE[c]	AdSDPV	0.02−1.67	0.0007	8
MCP-MWCNT/CPE[d]	SWV	0.5−1340	0.110	9
DMSA/Fe₃O₄/RGO/CNT	SWV	1−50	0.54	this work

[a]BDD—boron-doped diamond electrode. [b]ABSA/SWNT/GCE—aminobenzene sulfonic acid/single-wall carbon nanotubes/glassy carbon electrode. [c]MWCN T/GCE—multiwalled carbon nanotubes/glassy carbon electrode. [d]MCP-MWCNT/CPE—*m*-cresol purple-MWCNT-carboxylated multiwalled carbon nanotubes/carbon paste electrode.

DOP + Glu), resembling possible interfering molecules (Figure 6). The measured concentration ratios between TFP
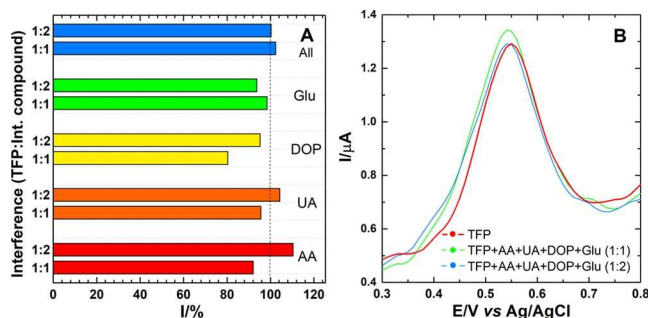

Figure 6. (A) Electrochemical response of TFP (10 μM) at the DMSA/Fe₃O₄/RGO/CNT electrode in the presence of interfering compounds: ascorbic acid (AA), uric acid (UA), dopamine (DOP), and glucose (Glu) at concentration ratios 1:1 and 1:2 v/v under optimized experimental conditions; (B) SWVs of the interference of all compounds combined.

(10 μM) and the molecules analyzed for interference in all examined conditions were 1:1 and 1:2. It was found that only DOP reduced the oxidation current for TFP slightly to 80% under the selected electrochemical window. The difference between interfered peaks was about 135 mV. In all other situations, the changes in current were significantly less than 10%. The electrochemical response in the presence of interfering compounds is summarized in Figure 6A, and the original SWV data are displayed in Figure S4. The presence of all four interfering compounds in a 2:1 ratio with the tested analyte does not interfere with the peak, and resulting currents were less than 10% different, as exhibited in Figure 6B. Based on these results, it can be concluded that the established procedure could be considered as highly selective for the detection of trifluoperazine and potentially usable for the determination of this drug when present in biological fluids.

Analysis of the Real Samples. To evaluate the detectability of TFP using the DMSA/Fe₃O₄/RGO/CNT sensor in actual testing, the standard recovery method was used to quantitatively analyze real urine and blood serum samples (Figure S5). The practical applicability of the procedure was investigated in four urine as well as two blood serum samples. The samples were processed following one of our previous works.[45] The recovery rates were investigated by two standard additions of TFP solution. Results were calculated from the calibration plots with three repetitive measurements and are summarized in Table 2. The recovery rates of the tested urine samples were in the range of 97.8−101.6%, bias values were between −0.8 and 1.8%, and the RSD values were in the range of 2.1−3.5%. As for the blood serum tests, recovery rates were 98.9−101.5%, the bias values were in the range of −1.7 to 1.9%, and the RSD values were between 2.1 and 3.1%. The given values are the indicators of the accuracy of the method. These results demonstrate that the proposed DMSA/Fe₃O₄/RGO/CNT sensor possesses good reliability and feasibility for the detection of TFP in human urine and blood serum samples.

■ CONCLUSIONS

Using inkjet printing for highly reproducible CNT electrode fabrication and newly synthesized DMSA/Fe₃O₄/RGO nanocomposite for the electrode surface modification, an electrochemical sensor for the determination of trifluoperazine in biological fluids has been developed. A disposable, flexible, fast, and easy-to-use sensor expressed a wide linear range of 1−50 μM, a submicromolar limit of detection of 0.54 μM, and excellent reproducibility and accuracy with a negligible influence of potently interfering compounds. The results of this study provide new possibilities for the production of advanced miniature electrochemical devices for the droplet-based detection of antipsychotic drug trifluoperazine founded on the utilization of state-of-the-art approaches. The future work will be directed toward the development of a portable

Table 2. Recovery Data for Spiked Human Urine and Blood Serum Samples Using DMSA/Fe₃O₄/RGO/CNT Sensor

			addition 1			addition 2			
				detected			detected		
	sample	detected (μM)	added[a] (μM)	bias (%)	RSD (%)	added[a] (μM)	bias (%)	RSD (%)	recov. (%)
urine	1	0.00	5.00	1.8	3.0	5.00	1.6	3.5	101.60
	2	0.00	5.00	−1.6	2.4	5.00	−1.2	2.6	97.80
	3	0.00	10.00	−1.1	2.1	10.00	−0.8	2.2	99.10
	4	0.00	10.00	−1.4	2.7	10.00	−1.6	2.8	98.40
blood serum	1	0.00	5.00	−1.7	2.8	5.00	−1.9	3.1	98.9
	2	0.00	10.00	0.9	2.3	10.00	1.5	2.9	101.50

[a]Average of three replicate measurements.

"on body" sensing devices and the transformation of the sensor for potential on body applications. This perspective with excellent sensing properties may replace other more complicated and expensive methods in the near future.

■ ASSOCIATED CONTENT

✱ Supporting Information

Cyclic voltammograms of bare and modified CTN electrodes at various scan rates; electrochemical response of 10 μM of TFP under the same SWV conditions; electrochemical response of TFP in the presence of different interfering compounds; and calibration plots used for real-sample analysis.

AUTHOR INFORMATION

Corresponding Author

Miloš Ognjanović − The "Vinča Institute of Nuclear Sciences, University of Belgrade, 11001 Belgrade, Serbia; orcid.org/0000-0003-2889-4416; Email: miloso@vin.bg.ac.rs

Authors

Dalibor M. Stanković − The "Vinča Institute of Nuclear Sciences, University of Belgrade, 11001 Belgrade, Serbia; orcid.org/0000-0001-7465-1373

Milica Jović − Laboratory of Physical and Analytical Electrochemistry (LEPA), EPFL Valais Wallis, CH-1951 Sion, Switzerland

Milena P. Krstić − Faculty of Veterinary Medicine, University of Belgrade, 11000 Belgrade, Serbia

Andreas Lesch − Department of Industrial Chemistry "Toso Montanari", University of Bologna, 40136 Bologna, Italy; orcid.org/0000-0002-4995-2251

Hubert H. Girault − Laboratory of Physical and Analytical Electrochemistry (LEPA), EPFL Valais Wallis, CH-1951 Sion, Switzerland; orcid.org/0000-0001-5573-5774

Bratislav Antić − The "Vinča Institute of Nuclear Sciences, University of Belgrade, 11001 Belgrade, Serbia

Author Contributions

The manuscript was written through contributions of all authors

Notes

The authors declare no competing financial interest.

■ ACKNOWLEDGMENTS

■ REFERENCES

(1) Hassan, A. K.; Ameen, S. T.; Saad, B.; Al-Aragi, S. M. Potentiometric Sensors for the Determination of Trifluoperazine Hydrochloride in Pharmaceutical Preparations. *Anal. Sci.* 2009, *25*, 1295−1299.

(2) Gao, K.; Muzina, D.; Gajwani, P.; Calabrese, J. R. Efficacy of typical and atypical antipsychotics for primary and comorbid anxiety symptoms or disorders: a review. *J. Clin. Psychiatry* 2006, *67*, 1327−1340.

(3) Yeh, C.-T.; Wu, A. T. H.; Chang, P. M.-H.; Chen, K.-Y.; Yang, C.-N.; Yang, S.-C.; Ho, C.-C.; Chen, C.-C.; Kuo, Y.-L.; Lee, P.-Y.; et al. Trifluoperazine, an antipsychotic agent, inhibits cancer stem cell growth and overcomes drug resistance of lung cancer. *Am. J. Respir. Crit. Care Med.* 2012, *186*, 1180−1188.

(4) Srinivasan, S.; Chizmadzhev, Y. A.; Bockris, J. O.'M.; Conway, B. E.; Yeager, E. *Comprehensive Treatise of Electrochemistry*; Springer US: Boston, MA, 1985.

(5) *The United States Pharmacopeia: USP 24: the National Formulary: NF 19: by authority of the United States Pharmacopoeial Convention, Inc., meeting at Washington, D.C., March 9-12, 1995; prepared by the Committee of Revision and published by the Board of Trustees*; United States Pharmacopeial Convention: Rockville, Md., 1999.

(6) Stanković, D.; Dimitrijević, T.; Kuzmanović, D.; Krstić, M. P.; Petković, B. B. Voltammetric determination of an antipsychotic agent trifluoperazine at a boron-doped diamond electrode in human urine. *RSC Adv.* 2015, *5*, 107058−107063.

(7) Jin, G.; Huang, F.; Li, W.; Yu, S.; Zhang, S.; Kong, J. Sensitive detection of trifluoperazine using a poly-ABSA/SWNTs film-modified glassy carbon electrode. *Talanta* 2008, *74*, 815−820.

(8) Dogan-Topal, B. Electrooxidative behavior and determination of trifluoperazine at multiwalled carbon nanotube-modified glassy carbon electrode. *J. Solid State Electrochem.* 2013, *17*, 1059−1066.

(9) Mohamed, M. A.; Saad, A. S.; Koshek, S. H.; El-Ghobashy, M. R. Smart electrochemical sensing platform for the simultaneous determination of psychotic disorder drugs isopropamide iodide and trifluoperazine hydrochloride. *New J. Chem.* 2018, *42*, 9911−9919.

(10) Muain, M. F. A.; Cheo, K. H.; Omar, M. N.; Amir Hamzah, A. S.; Lim, H. N.; Salleh, A. B.; Tan, W. S.; Ahmad Tajudin, A. Gold nanoparticle-decorated reduced-graphene oxide targeting anti hepatitis B virus core antigen. *Bioelectrochemistry* 2018, *122*, 199−205.

(11) Georgakilas, V.; Perman, J. A.; Tucek, J.; Zboril, R. Broad family of carbon nanoallotropes: classification, chemistry, and applications of fullerenes, carbon dots, nanotubes, graphene, nano-diamonds, and combined superstructures. *Chem. Rev.* 2015, *115*, 4744−4822.

(12) Jariwala, D.; Sangwan, V. K.; Lauhon, L. J.; Marks, T. J.; Hersam, M. C. Carbon nanomaterials for electronics, optoelectronics, photovoltaics, and sensing. *Chem. Soc. Rev.* 2013, *42*, 2824−2860.

(13) Bahadır, E. B.; Sezgintürk, M. K. Applications of graphene in electrochemical sensing and biosensing. *TrAC, Trends Anal. Chem.* 2016, *76*, 1−14.

(14) Rather, J. A.; Pilehvar, S.; Wael, K. de. A graphene oxide amplification platform tagged with tyrosinase−zinc oxide quantum dot hybrids for the electrochemical sensing of hydroxylated polychlorobiphenyls. *Sens. Actuators, B* 2014, *190*, 612−620.

(15) Georgakilas, V.; Tiwari, J. N.; Kemp, K. C.; Perman, J. A.; Bourlinos, A. B.; Kim, K. S.; Zboril, R. Noncovalent Functionalization of Graphene and Graphene Oxide for Energy Materials, Biosensing, Catalytic, and Biomedical Applications. *Chem. Rev.* 2016, *116*, 5464−5519.

(16) Ding, D.; Maeyoshi, Y.; Kubota, M.; Wakasugi, J.; Kanamura, K.; Abe, H. Highly improved performances of LiMn0.7Fe0.3PO4 cathode with in situ electrochemically reduced graphene oxide. *J. Alloys Compd.* 2019, *793*, 627−634.

(17) Hasanzadeh, M.; Shadjou, N.; La Guardia, M. de. Iron and iron-oxide magnetic nanoparticles as signal-amplification elements in electrochemical biosensing. *TrAC, Trends Anal. Chem.* 2015, *72*, 1−9.

(18) He, J.; Yang, X.; Men, B.; Wang, D. Interfacial mechanisms of heterogeneous Fenton reactions catalyzed by iron-based materials: A review. *J. Environ. Sci.* 2016, *39*, 97−109.

(19) Mohammed, L.; Gomaa, H. G.; Ragab, D.; Zhu, J. Magnetic nanoparticles for environmental and biomedical applications: A review. *Particuology* 2017, *30*, 1−14.

(20) Zhang, L.; Wang, X.; Zou, J.; Liu, Y.; Wang, J. DMSA-Coated Iron Oxide Nanoparticles Greatly Affect the Expression of Genes

Coding Cysteine-Rich Proteins by Their DMSA Coating. *Chem. Res. Toxicol.* 2015, *28*, 1961−1974.

(21) Ghalehno, M. H.; Mirzaei, M.; Torkzadeh-Mahani, M. Double strand DNA-based determination of menadione using a Fe3O4 nanoparticle decorated reduced graphene oxide modified carbon paste electrode. *Bioelectrochemistry* 2018, *124*, 165−171.

(22) Su, X.; Chan, C.; Shi, J.; Tsang, M.-K.; Pan, Y.; Cheng, C.; Gerile, O.; Yang, M. A graphene quantum dot@Fe3O4@SiO2 based nanoprobe for drug delivery sensing and dual-modal fluorescence and MRI imaging in cancer cells. *Biosens. Bioelectron.* 2017, *92*, 489−495.

(23) Stanković, D. M.; Ognjanović, M.; Espinosa, A.; del Puerto Morales, M.; Bessais, L.; Zehani, K.; Antić, B.; Dojcinović, B. Iron Oxide Nanoflower−Based Screen Print Electrode for Enhancement Removal of Organic Dye Using Electrochemical Approach. *Electrocatalysis* 2019, *74*, 239.

(24) Wang, Q.; Zhang, X.; Huang, L.; Zhang, Z.; Dong, S. One-pot synthesis of Fe3O4 nanoparticle loaded 3D porous graphene nanocomposites with enhanced nanozyme activity for glucose detection. *ACS Appl. Mater. Interfaces* 2017, *9*, 7465−7471.

(25) Aydogdu, M. O.; Ekren, N.; Suleymanoglu, M.; Erdem-Kuruca, S.; Lin, C.-C.; Bulbul, E.; Erdol, M. N.; Oktar, F. N.; Terzi, U. K.; Kilic, O. Novel electrospun polycaprolactone/graphene oxide/Fe3O4 nanocomposites for biomedical applications. *Colloids Surf., B* 2018, *172*, 718−727.

(26) Jarosŏvá, R.; Mcclure, S. E.; Gajda, M.; Jović, M.; Girault, H. H.; Lesch, A.; Maiden, M.; Waters, C.; Swain, G. M. Inkjet-Printed Carbon Nanotube Electrodes for Measuring Pyocyanin and Uric Acid in a Wound Fluid Simulant and Culture Media. *Anal. Chem.* 2019, *91*, 8835−8844.

(27) Lesch, A.; Cortés Salazar, F.; Amstutz, V.; Tacchini, P.; Girault, H. H. Inkjet printed nanohydrogel coated carbon nanotubes electrodes for matrix independent sensing. *Anal. Chem.* 2015, *87*, 1026−1033.

(28) Qin, Y.; Kwon, H.-J.; Subrahmanyam, A.; Howlader, M. M. R.; Selvaganapathy, P. R.; Adronov, A.; Deen, M. J. Inkjet-printed bifunctional carbon nanotubes for pH sensing. *Mater. Lett.* 2016, *176*, 68−70.

(29) Azoubel, S.; Shemesh, S.; Magdassi, S. Flexible electroluminescent device with inkjet-printed carbon nanotube electrodes. *Nanotechnology* 2012, *23*, No. 344003.

(30) Stanković, D. M.; Ognjanović, M.; Jović, M.; Cuplić, V.; Lesch, A.; Girault, H. H.; Gavrović Jankulović, M.; Antić, B. Disposable Biosensor Based on Amidase/CeO2/GNR Modified Inkjet-printed CNT Electrodes-droplet Based Paracetamol Detection in Biological Fluids for "Point-of-care" Applications. *Electroanalysis* 2019, *31*, 1517−1525.

(31) Stanković, D. M.; Jović, M.; Ognjanović, M.; Lesch, A.; Fabiań, M.; Girault, H. H.; Antić, B. Point-of-care amperometric determination of L-dopa using an inkjet-printed carbon nanotube electrode modified with dandelion-like MnO2 microspheres. *Mikrochim. Acta* 2019, *186*, No. 532.

(32) Salas, G.; Casado, C.; Teran, F. J.; Miranda, R.; Serna, C. J.; Morales, M. P. Controlled synthesis of uniform magnetite nanocrystals with high-quality properties for biomedical applications. *J. Mater. Chem.* 2012, *22*, No. 21065.

(33) Mejías, R.; Pérez-Yagüe, S.; Gutiérrez, L.; Cabrera, L. I.; Spada, R.; Acedo, P.; Serna, C. J.; Lázaro, F. J.; Villanueva, A.; Morales, M. D. P.; et al. Dimercaptosuccinic acid-coated magnetite nanoparticles for magnetically guided in vivo delivery of interferon gamma for cancer immunotherapy. *Biomaterials* 2011, *32*, 2938−2952.

(34) Lu, T.; Pan, L.; Nie, C.; Zhao, Z.; Sun, Z. A green and fast way for reduction of graphene oxide in acidic aqueous solution via microwave assistance. *Phys. Status Solidi A* 2011, *208*, 2325−2327.

(35) Schneider, C. A.; Rasband, W. S.; Eliceiri, K. W. NIH Image to ImageJ: 25 years of image analysis. *Nat. Methods* 2012, *9*, 671.

(36) Jović, M.; Zhu, Y.; Lesch, A.; Bondarenko, A.; Cortés Salazar, F.; Gumy, F.; Girault, H. H. Inkjet-printed microtiter plates for portable electrochemical immunoassays. *J. Electroanal. Chem.* 2017, *786*, 69−76.

(37) Lesch, A.; Cortés Salazar, F.; Prudent, M.; Delobel, J.; Rastgar, S.; Lion, N.; Tissot, J.-D.; Tacchini, P.; Girault, H. H. Large scale inkjet-printing of carbon nanotubes electrodes for antioxidant assays in blood bags. *J. Electroanal. Chem.* 2014, *717−718*, 61−68.

(38) Lesch, A.; Jović, M.; Baudoz, M.; Zhu, Y.; Tacchini, P.; Gumy, F.; Girault, H. H. (Invited) Point-of-Care Diagnostics with Inkjet-Printed Microchips. *ECS Trans.* 2017, *77*, 73−81.

(39) Jović, M.; Cortés Salazar, F.; Lesch, A.; Amstutz, V.; Bi, H.; Girault, H. H. Electrochemical detection of free chlorine at inkjet printed silver electrodes. *J. Electroanal. Chem.* 2015, *756*, 171−178.

(40) Mehmeti, E.; Stanković, D. M.; Chaiyo, S.; Zavasnik, J.; Žagar, K.; Kalcher, K. Wiring of glucose oxidase with graphene nanoribbons: an electrochemical third generation glucose biosensor. *Microchim. Acta* 2017, *184*, 1127−1134.

(41) Lu, S.; Sui, L.; Liu, J.; Zhu, S.; Chen, A.; Jin, M.; Yang, B. Near-Infrared Photoluminescent Polymer-Carbon Nanodots with Two-Photon Fluorescence. *Adv. Mater.* 2017, *29*, No. 1603443.

(42) Sun, S.; Guan, Q.; Liu, Y.; Wei, B.; Yang, Y.; Yu, Z. Highly luminescence manganese doped carbon dots. *Chin. Chem. Lett.* 2019, *30*, 1051−1054.

(43) Huízar-Félix, A. M.; Cruz-Silva, R.; Barandiarań, J. M.; García-Gutiérez, D. I.; Orue, I.; Merida, D.; Sepúlveda-Guzmań, S. Magnetic properties of thermally reduced graphene oxide decorated with PtNi nanoparticles. *J. Alloys Compd.* 2016, *678*, 541−548.

(44) Stanković, D. M.; Ognjanović, M.; Martin, F.; Svorc, L'.; Mariano, J. F. M. L.; Antić, B. Design of titanium nitride- and wolfram carbide-doped RGO/GC electrodes for determination of gallic acid. *Anal. Biochem.* 2017, *539*, 104−112.

(45) Vukojević, V.; Djurdjić, S.; Ognjanović, M.; Antić, B.; Kalcher, K.; Mutić, J.; Stanković, D. M. RuO2/graphene nanoribbon composite supported on screen printed electrode with enhanced electrocatalytic performances toward ethanol and NADH biosensing. *Biosens. Bioelectron.* 2018, *117*, 392−397.